Journal of Inflammation Research

Dovepress
Taylor & Francis Group

Open Access Full Text Article

ORIGINAL RESEARCH

Potential Targets and Bioactive Constituents of Daying Decoction in Schizophrenia with Neuroinflammation: A Preliminary Exploratory Integrative Study

Lina Guo[1,*], Bilin Zhang[1,*], Meiying Liu[1,*], Yuxi Qin[1], Hongxiao Lu[1], Ze Wang[1], Yiting Yuan[1], Qian Zheng[1], Guang Zhao[1], Yanan Qiao[3], Ruodi Ma[4], Bocheng Lu[2], Yunlan Li[1]

[1]School of Pharmaceutical Science, Shanxi Medical University, Taiyuan, 030001, People's Republic of China; [2]Traditional Chinese Medicine Innovation team of Shanxi Traditional Chinese Medicine Administration, Shanxi Hospital of Traditional Chinese Medicine, Taiyuan, 030001, People's Republic of China; [3]Department of Pharmacy, Second hospital of Shanxi Medical University, Taiyuan, 030001, People's Republic of China; [4]School of Basic Medical Sciences, Tongji Medical College, Huazhong University of Science and Technology, Wuhan, 430030, People's Republic of China

*These authors contributed equally to this work

Correspondence: Yunlan Li, School of Pharmaceutical Science, Shanxi Medical University, 56 Xinjian South Road, Taiyuan, 03000, People's Republic of China, Email liyunlan@sxmu.edu.cn; Bocheng Lu, Shanxi Hospital of Traditional Chinese Medicine, Taiyuan, 030001, People's Republic of China, Email lubocheng0523@163.com

Purpose: Schizophrenia (SZ) is a serious disorder often linked to schizophrenia-related neuroinflammation (SZNI). While second-generation antipsychotics (SGAs) are available, their metabolic side effects highlight the need for alternative therapies. The traditional Chinese medicine compound Daying Decoction (DYD) has shown good clinical efficacy in the treatment of SZNI, but its molecular mechanisms and pharmacological targets are not well understood. There are also no studies that have yet reported their interaction with SZNI.

Methods: To find out how DYD might help with SZNI, we used bioinformatics tools to analyze things like gene activity, immune cell presence, and key gene patterns. We also did lab tests—including molecular docking, molecular dynamics simulation, and experiments in cell cultures—to check how the main active parts of DYD affect important genes.

Results: We identified, through bioinformatics analysis, that the transcription factor c-JUN may act as a key regulator in SZNI, and that rhein may serve as a core component. Molecular dynamics simulations and CETSA further confirmed the substantial structural stability of the c-JUN-Rhein complex. Finally, in vitro analyses indicated that rhein effectively reduced ROS levels and modulated neuroinflammatory biomarkers by inhibiting JNK/c-JUN phosphorylation and inflammatory factors.

Conclusion: We conducted the first comprehensive study of DYD against SZNI, identifying that c-JUN might represent a candidate that could be explored as a potential therapeutic target and that rhein may contribute as a core active component. This serves as a starting point that can guide future in vivo studies and the development of potential small-molecule therapies for SZNI.

Keywords: schizophrenia-related neuroinflammation, Traditional Chinese Medicine, bioinformatics, machine learning, molecular docking, molecular dynamics simulation

Introduction

Schizophrenia (SZ) is a complex heritable disease with long-term disease progression, possible disability, and treatment difficulties, taking a cost toll on patients' families and society.[1] Even with all the global efforts to figure out how it works, we still do not know its exact causes or mechanisms. Currently, the main drugs used are second-generation antipsychotics (SGAs), which primarily act by blocking 5-HT and dopamine receptors. However, they carry a high risk of metabolic side effects,[2] which might potentially lead to type 2 diabetes, cardiovascular diseases, and obesity. Furthermore, SGAs

Received: 2 June 2025
Accepted: 9 October 2025
Published: 22 October 2025

Graphical Abstract

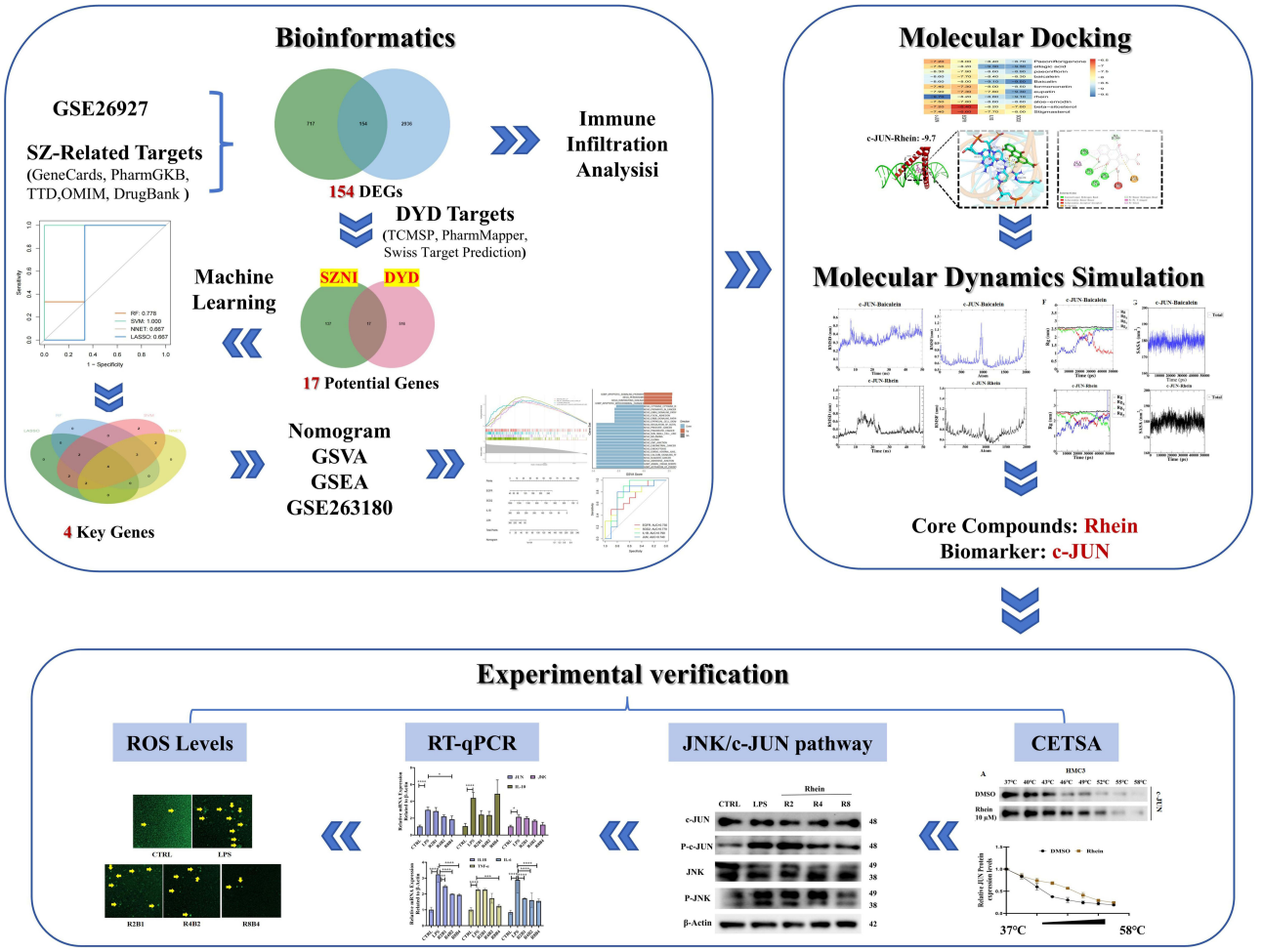

can also induce drug dependence with long-term use, with abrupt discontinuation often triggering withdrawal symptoms.[3,4]

TCM looks at health from a whole-body perspective. It sees SZ not just as a brain disorder but as a problem with multiple organ systems.[5] Because of the long-term clinical practice, TCM has shown encouraging efficacy on SZ with fewer side effects than traditional pharmacology.[6] Recently, it has been recognized for its possible therapeutic benefits.[7] Daying Decoction (DYD) is safe and effective in the treatment of chronic SZ and has been widely used in China as a TCM prescription for SZ[8,9] since it was first presented at the Academic Conference for Neurology and Psychiatry Division of Chinese Medical Association of Shanghai Branch on March 22, 1978. It was the first to clearly document that DYD was clinically effective in 40 out of 44 patients with cyclic psychosis, laying a clinical foundation for the subsequent promotion of this formula.[8] The formula is composed of 4 herbs: *Sparganium stoloniferum* Buch.-Ham. (60 g), *Curcuma phaeocaulis* Val. (60 g), *Paeonia lactiflora* Pall. (30 g), and *Rheum palmatum* L. (30 g). The synergy of these 4 medicinal herbs plays a significant role in DYD's clinical effectiveness in activating blood circulation, resolving blood stasis, and calming the mind. However, the active ingredients and molecular targets of DYD are still unknown. Most TCM studies stop at clinical descriptions and rarely dig into molecular pathways, leaving a clear gap. This makes it urgent and reasonable to carry out mechanistic studies.

Individuals with SZ frequently display low to moderate systemic inflammation.[10] Ongoing neuro-immune activation may give rise to a progressive wave of neuropathological alterations, such as neuronal apoptosis[11] and neuro-cognitive impairment.[12] In extreme cases, chronic neuroinflammation may result in systemic inflammation with increased risk of multi-organ failure and other conditions.[13] DYD is abundant in bioactive compounds with anti-inflammatory and antioxidant properties that may contribute to the reduction of neuroinflammation. For instance, paeoniflorigenone, a filter of the major compound of *Paeonia lactiflora*, can relieve neuroinflammation, oxidative stress, and cell death.[14] Similarly, one active component of *Sparganium stoloniferum*, formononetin, has been demonstrated to prevent neuroinflammation and exert tissue- and receptor-selective neuroprotective activity.[15] Currently, there are only reports on the clinical therapeutic effects of DYD with no research on its mechanisms or components.[9] Therefore, it is necessary to investigate DYD from a mechanistic perspective. Advances in machine learning offer powerful tools to integrate heterogeneous biomedical data, uncover latent associations, and predict functional components and pathways with high accuracy.[16,17] When applied in combination with network pharmacology and transcriptomic analysis, these approaches enable a systematic and objective evaluation of complex herbal formulas such as DYD. This integrated strategy not only enhances the reliability of TCM research but also provides a means to transform traditional empirical knowledge into evidence-based mechanistic insights.

In the current landscape, there is a pressing need to clarify the pharmacological mechanisms underlying the therapeutic efficacy of DYD in SZNI. To address this, we designed a study that integrates bioinformatics analysis, public databases, and network pharmacology, in combination with molecular docking, molecular dynamics simulations, and preliminary in vitro validation. This integrative strategy was intended to generate hypotheses and provide a systematic framework for understanding the potential molecular basis of DYD in SZNI. This study aims to reveal the underlying molecular mechanisms of DYD's neuroprotective effects. It also seeks to identify the major active components, possible therapeutic targets, and related signal pathways through which DYD alleviates neuroinflammation in patients with SZ. These efforts are intended to provide a preliminary basis for generating hypotheses regarding its clinical application (Graphical abstract).

Materials and Methods

Obtain the Dataset and Filter for Differentially Expressed Genes (DEGs)

This study performed the analysis of dataset GPL6255, publicly available in the GEO database (https://www.ncbi.nlm.nih.gov/geo/), with the GSE26927.[18] This includes data for six diseases pertaining to the central nervous system and neurodegeneration. After rigorous screening of the dataset and removal of samples with confounding phenotypes, we conducted statistical analyses comparing the control group and the SZNI group (with 10 replicate samples in each group). DEGs were analyzed with the GEO2R application, by estimating potential DEGs using the following cut-off criteria: adjusted p-value < 0.05 and absolute $\log_2 Fold\ Change$ ($\log_2 FC$) > 1.0. A volcano plot was marked by using dplyr and ggplot2 packages in R. The reproducibility analysis of GSE26927 data was validated with PCA data.

Identification of SZ-Associated Targetable Targets with Interference in Genes Associated with Neuroinflammation

The information related to these targets associated with SZ was extracted from multiple databases, including GeneCards (https://www.genecards.org/), PharmGKB (https://www.pharmgkb.org/), TTD (https://db.idrblab.net/ttd/), DrugBank (https://go.drugbank.com/) and OMIM (https://omim.org) using the keyword "schizophrenia". Only targets associated with a relevance score of 1 or above were included in the GeneCards database. Targets of interest were collated, and duplicates were removed. To determine the genes that overlap between DEGs relating to neuroinflammation and schizophrenia-related targets, a Venn diagram and a heatmap were created using an online bioinformatics tool.

Assessment of Immune Infiltration

The proportion of 22 immune cell types infiltration levels in each sample was evaluated based on the intersection genes by using the CIBERSORT package. Bar plots were created which showed the proportions of different immune cell types

in the different samples. We then used box plots to compare the abundance of the 22 immune cell types between control and SZNI groups. Additionally, immune cell types were extracted and visualized using the ggplot2 package.

Screening active Compounds and Presuming Potential Targets for DYD

The active ingredients of DYD were screened by using the Traditional Chinese Medicine Systems Pharmacology Database and Analysis Platform (TCMSP, https://tcmspw.com/tcmsp.php) with the following 2 screening criteria: oral bioavailability (OB) ≥ 30% and drug-likeness (DL) ≥ 0.18. Supplemental data for target identification of DYD came from the PharmMapper and Swiss Target Prediction platforms. The target data were integrated and duplicate records removed, while species were limited to "*Homo sapiens*". The target information of DYD and the SZNI-related intersecting genes was separately imported to construct a Venn diagram using the Bioinformatics online platform.

PPI, GO, KEGG Analysis and Construction of the Core Component-Potential Target-Signaling Pathway Network (CPSN)

Using the STRING database and Cytoscape 3.10.1 software, we visualized the PPI network of potential targets. The topological analysis of the PPI network was conducted using the CytoNCA plugin, and the degree values were calculated. A PPI network diagram was built. Next, the potential targets underwent GO and KEGG pathway enrichment analyses. The top 15 enriched signaling pathways, including their targets and core components, were imported into Cytoscape to construct the CPSN.

Selecting Hub Genes Using Machine Learning

To identify hub genes associated with SZNI, 4 machine learning models were applied: Least Absolute Shrinkage and Selection Operator (LASSO), Support Vector Machine (SVM), Random Forest (RF), and Neural Network (NNET, size = 2). To ensure the reproducibility of results, a random seed of 6666 was set; the mean squared error was used as the model evaluation metric, and leave-one-out cross-validation was employed to select the minimum lambda value, with the model corresponding to this value being the optimal one. Additionally, L1/L2 regularization was added and learning curves were plotted to alleviate overfitting of the data. The importance of features was first evaluated using the caret and DALEX R packages, applying 4 machine learning methods. The results were then visualized using ggplot2. Model predictions for potential genes were carried out using the glmnet, randomForest, e1071, and nnet packages in R. Genes with absolute coefficients greater than 0 were considered significant for further analysis. A Venn diagram was created to identify overlapping genes, and the final hub genes were selected from this intersection.

Construction of a Diagnostic Model and Evaluation of Hub Genes

A nomogram is a visualization tool that integrates multiple hub genes and represents them as line segments of different lengths on a single plane in proportion to their significance. This method is useful for illustrating relationships between variables in a diagnostic model.[19] The rms package in R was used to construct the nomogram and assess the significance of the hub genes.

Receiver operating characteristic (ROC) curves are commonly used to evaluate model performance by measuring sensitivity and specificity.[20] The accuracy of hub genes was analyzed using the pROC package in R, displaying the Area Under the Curve (AUC) values for each gene. A higher AUC indicates stronger model performance.[21]

Gene set variation analysis (GSVA) is an unsupervised method that assesses gene activity levels across samples or cell groups. In this study, the GSVA R package was used to perform pathway enrichment analysis for hub genes. Besides, single-gene set enrichment (GSEA) was conducted using the clusterProfiler R package and the org.hs.eg.db[22] database. Genes with significant associations ($p < 0.05$) were analyzed for C2 pathway enrichment (https://www.gsea-msigdb.org/gsea/msigdb/human/collections.jsp#C2).

Molecular Docking

Molecular docking is a computational tool for predicting ligand and target interactions and studying conformation changes at the molecular level. To gain deeper insights into the relationship between hub genes and their corresponding components, we focused on genes and components with high degree values. And then we treated them as core components. Molecular docking simulations were carried out using AutoDock software to confirm these interactions. The PDB files for the targets were obtained from the Protein Data Bank (PDB), and the MOL2 structures of active components were sourced from PubChem. Docking was performed in AutoDock after preprocessing, and the results were visualized using PyMOL version 4.6.0.

Molecular Dynamics (MD) Simulations

MD simulations were performed to gain a deeper understanding of the interaction strength and overall stability of the receptor-ligand complex. These simulations employ the Amber14sb force field alongside SPC water molecules to replicate physiological conditions.[23] The system was optimized for 50,000 steps using steepest descent and conjugate gradient algorithms. Equilibration took place in both NVT and NPT ensembles with a 2 fs time step over 50 ns. After equilibration, a 100 ns MD simulation was run at a constant temperature of 300 K. The trajectory was processed using GROMACS 2022.2 tools to generate the final structure at 100 ns, and this process was repeated three times. Key metrics, including root mean square deviation (RMSD), radius of gyration (RG), solvent-accessible surface area (SASA), and root mean square fluctuation (RMSF), were analyzed. Visualization was done using QtGrace version 5.0.

Experimental Verification

Cell Culture, Drugs and Reagents

BV2 cells were obtained from the Cell Bank of the Chinese Academy of Sciences (Shanghai, China) and used in this study were cultured in complete DMEM (Gibco, USA), supplemented with 10% fetal bovine serum (FBS) (CellMax, SA211.03, China), and 1% penicillin/streptomycin/Amphotericin B (MeilunBio, China). HMC3 cells were purchased from the Haixing Biosciences Co., Ltd (Jiangsu, China) and incubated in MEM medium, which is added with 10% FBS, and 1% penicillin/streptomycin.DEGs between the control and neuroinflammation groups were analyzed using the GEO2R online tool. Cells were kept in a humidified incubator at 37°C with 5% CO_2. Baicalein (Macklin, China, purity ≥ 98.0%) and rhein (Macklin, China, purity ≥ 98.0%) were dissolved in DMSO. The final DMSO concentration in the culture medium was kept below 0.1% to prevent toxicity. Neuroinflammation was induced by treating BV2 cells and HMC3 cells with 0.2 μg/mL lipopolysaccharide (LPS) for 24 hours.

Reagents used included the CCK-8 kit (WILBER, China), TRIzol reagent (Mei5bio, China), M5 Superr Plus qPCR RT Kit with gDNA remover (Mei5bio, China), 2×M5 Hiper SYBR Premix EsTaq (Mei5bio, China), primers (Sangon Biotech, China), BAC Protein Quantifier Kit (BOSTER, China), ROS Assay Kit (Beyotime, China, S0033S), Goat Anti-Rabbit IgG (H+L) (BOSTER, China, BA1054), and antibodies against AP-1 (c-JUN) Rabbit pAb (Immunoway, YT0251, USA), JNK1/2/3 Rabbit pAb (Immunoway, YT2440, USA), Anti-beta Actin Rabbit pAb (Servicebio, GB11001-100, China), P-c-JUN-S63 Rabbit mAb (ABclonal, AP0105, China), and P-JNK-T183/Y185 Rabbit mAb (ABclonal, AP1337, China).

Cell Viability Assay

Cell viability was measured using a CCK-8 assay. BV2 cells were seeded into a 96-well plate at a density of 3×10^3 cells per well in 100 μL of medium. Baicalein (0, 0.05, 0.1, 0.25, 0.5, 1, 2, 4, 5, 10, 20 and 30 μmol/L) and rhein (0, 1, 2, 5, 10, 15, 20, 30 and 40 μmol/L) were added after an overnight culture. 10 μL of CCK-8 reagent was added to each well after 24 hours. Then the plates were incubated for 1 hour. Absorbance was measured at 450 nm using a microplate reader.

Reverse Transcription Quantitative Polymerase Chain Reaction (RT-qPCR)

Baicalein and rhein were applied 2 hours before LPS exposure. After 26 hours of treatment, BV2 cells were washed with precooled PBS. TRIzol reagent was used to extract total RNA, and its purity and concentration were assessed using a microplate reader. RNA was reverse transcribed into cDNA using the M5 Superr Plus qPCR RT Kit. Gene amplification was performed using 2×M5 Hiper SYBR Premix EsTaq, following the manufacturer's protocol. Real-time PCR products

Table 1 Primer Sequences of RT-qPCR

Gene	Forward primer (5′-3′)	Reverse primer (5′-3′)
ACTB	TATGCTCTCCCTCACGCCATCC	GTCACGCACGATTTCCCTCTCAG
JUN	CTACGCCAACCTCAGCAACTTC	TGCGGCTGCGAGGGAAAG
JNK	GCAGAAGCCCCACCACCAAAG	ACGGCTGCCCTCTTATGACTCC
IL1B	GCAGCAGCACATCAACAAGAGC	AGGTCCACGGGAAAGACACAGG
IL-6	TTCTTGGGACTGATGCTGGTGAC	CTGTTGGGAGTGGTATCCTCTGTG
TNF-α	GCCACCACGCTCTTCTGTCTAC	GGTTTGTGAGTGTGAGGGTCTGG

were monitored, and cycle threshold (Ct) values were recorded. Gene expression was calculated using the $2^{-\Delta\Delta Ct}$ method.[24] Primer sequences for genes are listed in Table 1.

Western Blotting (WB)

Protein concentrations were determined using the BCA assay. Proteins were separated by SDS-PAGE (Servicebio, China) and transferred onto a 0.22 μm nitrocellulose (NC) membrane (Baseniao, China, BSN3303B). Membranes were blocked for 30 minutes, followed by overnight incubation at 4°C with primary antibodies against c-JUN (1:1300), P-c-JUN-S63 (1:1300), P-JNK-T183/Y185 (1:3000), and JNK1/2/3 (1:1300). Membranes were washed and incubated with a secondary antibody for 2 hours at room temperature. After washing, the membranes were developed with an ECL substrate. Repeat each protein three times. Band intensities were quantified using ImageJ software.

Reactive Oxygen Species (ROS) Assay

ROS levels were measured using the DCFH-DA probe. BV2 cells were seeded into 24-well plates and cultured for 24 hours. After removing the culture medium, 300 μL of 1:1000 diluted DCFH-DA was added to each well. Cells were incubated at 37°C for 25 minutes, then washed with serum-free medium. Fluorescence intensity was measured using a high-content automated cell imaging system (Molecular Device, USA, ImageXpress Pico) with excitation at 488 nm and emission at 525 nm for FITC.

Cellular Thermal Shift Assay (CETSA)

CETSA was used to study the protective effects of baicalein and rhein on c-JUN's thermal denaturation. Rhein (10 μM) and baicalein (4 μM) were added to cells and incubated at 37°C for 3 hours. Cells were washed with PBS, and the supernatant was collected. It was divided into eight portions and subjected to thermal denaturation at temperatures between 37°C and 58°C. After centrifugation, the supernatant was mixed with loading buffer and denatured at 100°C for 10 minutes before performing WB analysis. DMSO-treated cells were included as vehicle controls in all CETSA experiments.

Statistical Analysis

All experiments were conducted with three independent biological replicates, with data presented as mean ± SD. One-way ANOVA was used to assess statistical significance with Prism 10.3.1 software. A p-value < 0.05 was considered statistically significant.

Results

Screening of Overlapping Targets of SZNI, Pathway Enrichment Analysis, and Immune Infiltration Analysis

PCA showed high reproducibility in the GSE26927 dataset (Figure 1A).DEGs between the control and neuroinflammation groups were analyzed using the GEO2R online tool. A total of 871 DEGs were identified, including 474 upregulated and 397 downregulated genes, as shown in a volcano plot (Figure 1B).

To find overlapping genes, 2997 SZ-related targets were collected from the GeneCards database. Additional targets were included from OMIM (59 targets), PharmGKB (4 targets), TTD (52 targets), and DrugBank (139 targets), resulting

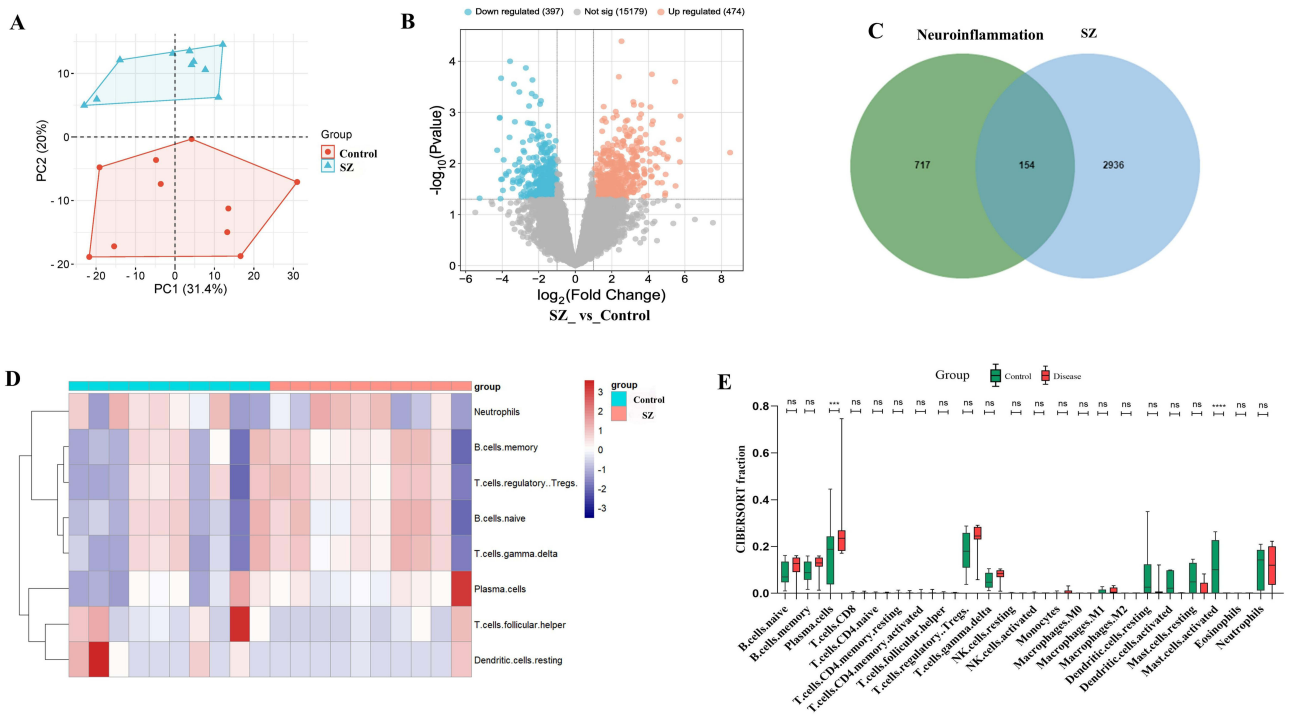

Figure 1 Screening of intersecting targets of SZNI, pathway enrichment analysis, and immune infiltration analysis. (**A**) Principal component analysis (PCA) of GSE26927. (**B**) 871 DEGs of volcano plot. (**C**) A Venn diagram revealed 154 intersecting genes. (**D**) An immune cells heatmap of immune infiltration analysis. (**E**) Boxplot analysis of immune infiltration analysis.

in a total of 3090 unique SZ-related targets. To explore the molecular mechanisms of SZNI, the 871 DEGs from GSE26927 were compared with the 3090 SZ-associated targets. A Venn diagram revealed 154 overlapping genes (Figure 1C). The log2FC of these intersecting genes was displayed in a cluster heatmap, with red indicating upregulation, blue indicating downregulation, and color intensity representing the magnitude of expression change (Figure S2).

Immune infiltration levels were evaluated using the CIBERSORT package. A heatmap showed significant differences in the relative proportions of most immune cells between the control and SZNI groups (Figure 1D). This indicated that altered immune cell activity might contribute to neuroinflammatory processes in SZ symptoms. Boxplot analysis of immune infiltration levels (Figure 1E) highlighted significant differences in plasma cells and activated mast cells between the control and SZNI groups. It could influence the development of cognitive, emotional, and behavioral symptoms in SZNI. No significant differences ($p > 0.05$) were observed in other immune cell types.

Screening of DEGs Related to SZNI and DYD, Pathway Enrichment, and Construction of a CPSN

Using the TCMSP database with criteria OB ≥ 30% and DL ≥ 0.18, 53 active components corresponding to 432 targets were identified. *Sparganium stoloniferum* contained 5 active components targeting 140 targets, *Curcuma phaeocaulis* had 3 active components targeting 24 targets, *Paeonia lactiflora* included 29 active components targeting 158 targets, and *Rheum palmatum* had 16 active components targeting 110 targets. Swiss Target Prediction identified 786 targets, and PharmMapper provided 257 additional targets. 533 unique targets were finally found after removing duplicates.

A Venn diagram showed that 17 DEGs related to SZNI overlapped with DYD targets (Figure 2A). A potential target PPI network was built using Cytoscape (Figure 2B). Based on degree values, the two key targets were interleukin-6 (IL-6) and epidermal growth factor receptor (EGFR). The Sankey bubble chart (KEGG, Figure 2C) revealed that the 17 potential targets were strongly linked to pathways like the "AGE-RAGE signaling pathway", "Lipid and Atherosclerosis", and "Th17 Cell Differentiation". GO enrichment analysis indicated that these targets were involved

https://doi.org/10.2147/JIR.S544162

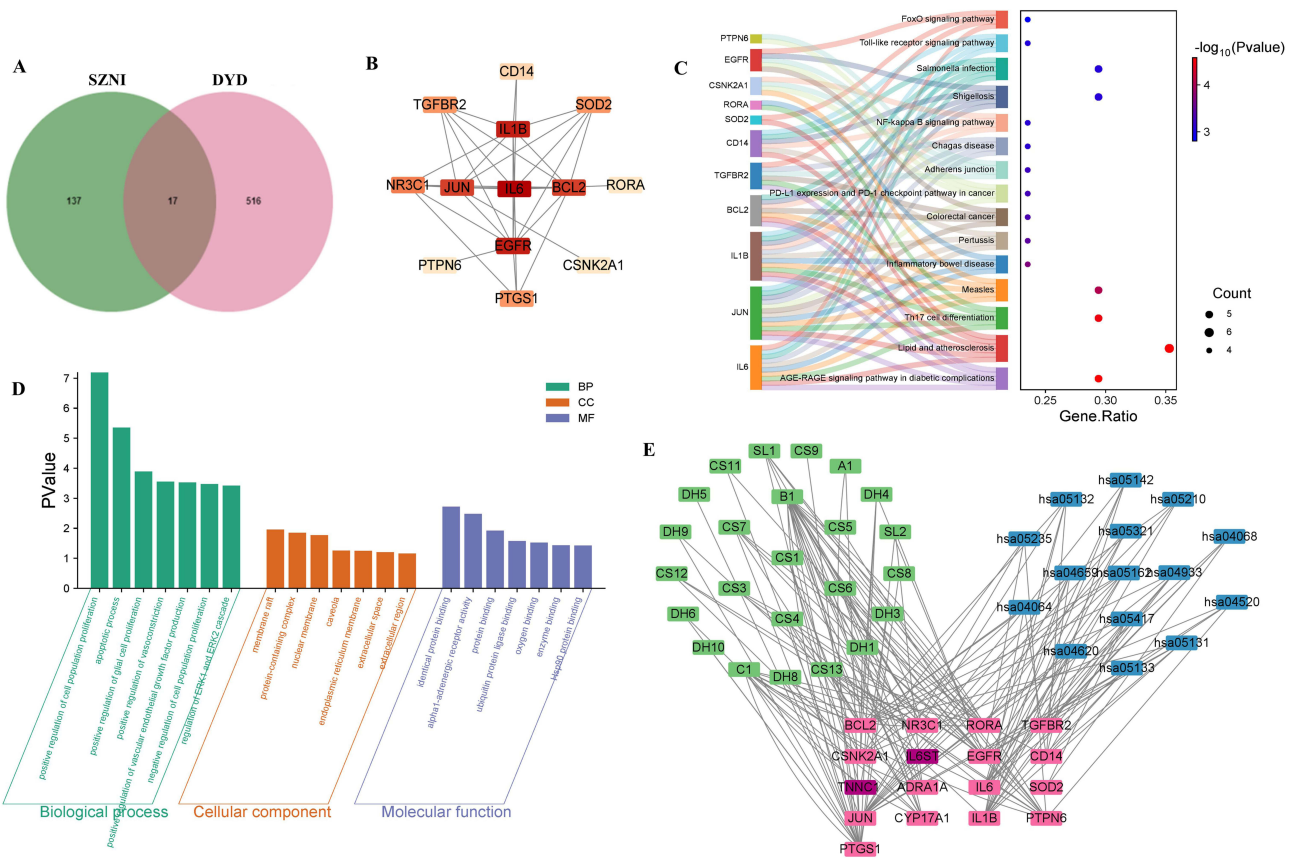

Figure 2 Screening of DEGs Associated with SZNI and 4 traditional herbs, Pathway Enrichment Analysis, and Construction of CPSN. (**A**) Venn diagram. (**B**) PPI network of potential targets. (**C**) Sankey bubble chart of 17 potential targets. (**D**) GO enrichment analysis revealed potential targets. (**E**) CPSN was constructed by mapping the 17 potential targets.

in cellular components (CC) such as membrane rafts and protein complexes, with molecular functions (MF) like protein binding and receptor activity. In biological processes (BP), 8 intersecting genes were involved in the positive regulation of cell proliferation, while 7 were involved in apoptosis (Figure 2D). A CPSN was then constructed by mapping the 17 potential targets, 24 core active components, and the top 15 ranked pathways (Figure 2E). JUN and IL1B appeared in 12 and 11 pathways respectively, which suggested they may be key therapeutic targets.

Machine Learning for Screening Hub Genes

To further investigate the hub genes involved in DYD's therapeutic effects on SZNI, 4 commonly used machine learning techniques were applied, and their model importance was systematically assessed.[19] Residual reverse cumulative distribution analysis showed that, at a probability of 100%, the absolute residuals for all 4 methods remained under 0.5, indicating low overall residual values and high model accuracy (Figure 3A). Boxplot analysis of the absolute residuals revealed that the LASSO method had the lowest residuals, suggesting its superior accuracy compared to the others (Figure 3B). ROC curve analysis showed that all 4 methods performed excellently in diagnostics, with AUC values well above the chance level (0.5, Figure 3C). A preliminary feature importance analysis was also conducted (Figure 3D).

Next, the 4 machine learning methods were used to analyze the 17 potential targets. We employed L1/L2 regularization and cross-validation methods, and the learning curves demonstrate that this approach reduces overfitting of the data (Figure S3). LASSO regression (Figure 4A and 4B) identified 10 genes—CYP17A1, TNNC1, PTGS1, CSNK2N1, BCL2, EGFR, JUN, IL1B, RORA, and SOD2—that showed significant differential expression between the control and disease groups (Supplementary Table S1). The SVM (Figure 4C and 4D) method identified all 17 genes (Supplementary Table S2), while

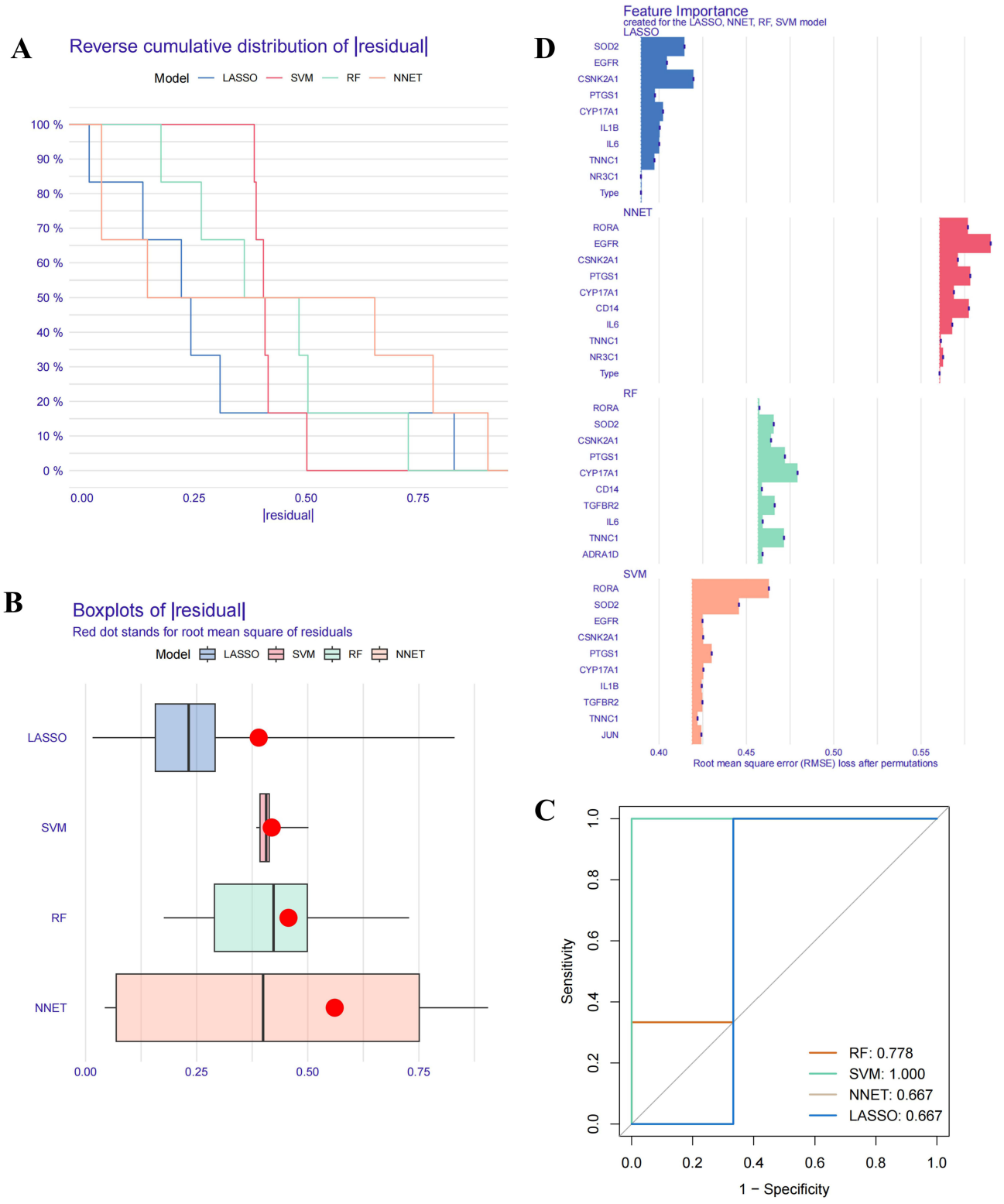

Figure 3 Four Machine learning methods. (**A**) The residual reverse cumulative distribution. (**B**) The absolute residual boxplot analysis. (**C**) ROC curve analysis. (**D**) Feature importance analysis.

https://doi.org/10.2147/JIR.S544162

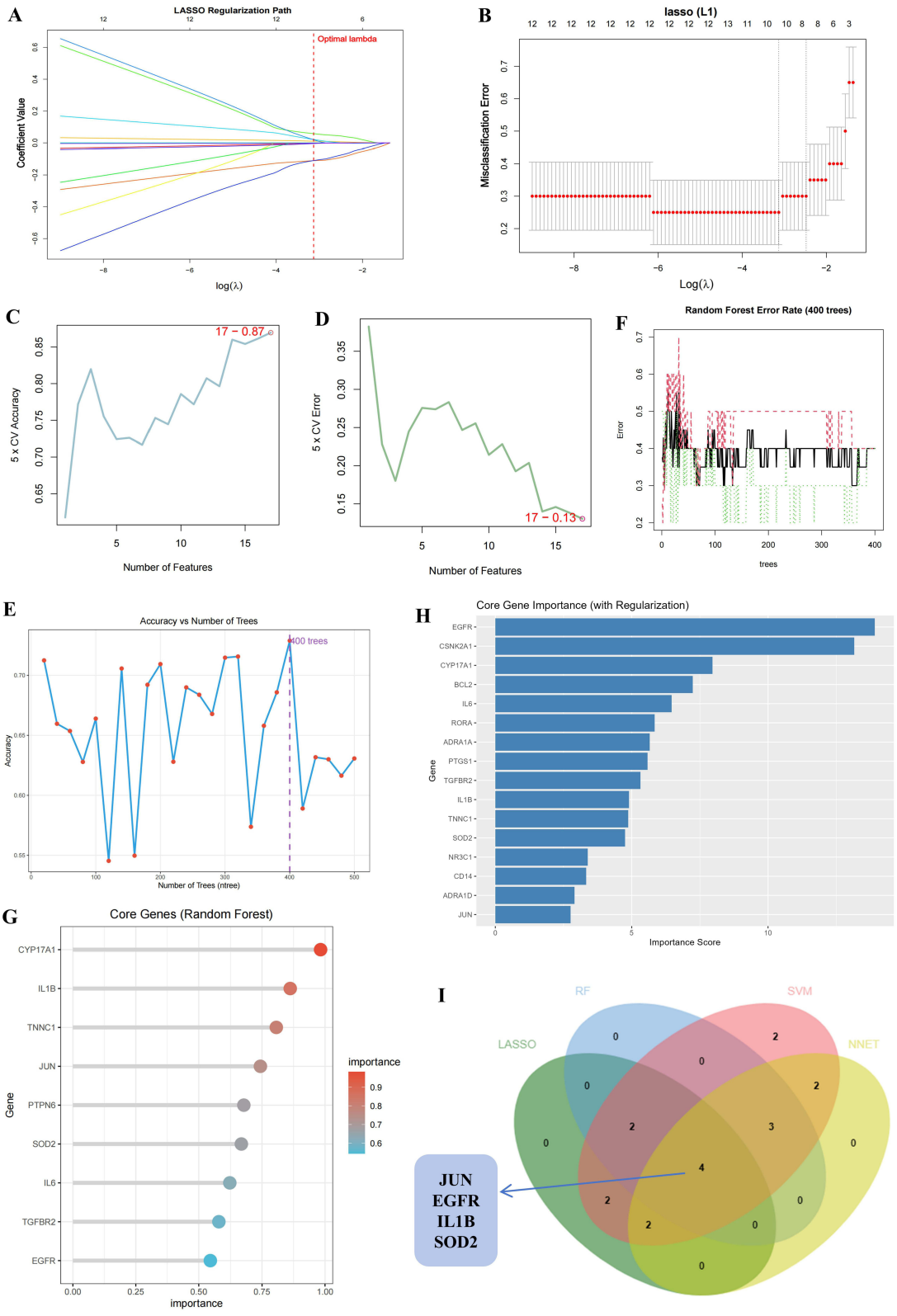

Figure 4 Machine learning for screening key genes. (**A**) Regression path diagram and (**B**) LASSO regression analysis cross-validation results. The SVM method includes the SVM Accuracy Plot (**D**) and SVM Error Rate Plot (**C**). The RF method's Evaluate the accuracy of different numbers of trees (**E**), error rate curve (**F**), and VIP evaluation (**G**). (**H**) The core genes of the NNET method. (**I**) A Venn diagram of key genes from the four machine learning methods.

the NNET method selected 9 core genes with an importance greater than 4 (Figure 4H): EGFR, JUN, RORA, ADRA1D, PTPN6, CSNK2N1, SOD2, TGFBR2, and CD14 (Supplementary Table S4). And for RF (Figure 4E–4G), the 400 trees with the highest accuracy were selected for cross-validation, resulting in 9 feature genes with a value greater than 0.5 (Supplementary Table S3). A Venn diagram showed the intersection of core genes identified by all 4 methods, resulting in the 4 hub genes: JUN, SOD2, EGFR, and IL1B (Figure 4I).

Construction of a Diagnostic Model and Evaluation of the 4 Hub Genes

A nomogram was created for the 4 hub genes (JUN, EGFR, IL1B, and SOD2) to evaluate their significance in the diagnostic model (Figure 5A). Each gene received an individual score, and the total score was calculated by summing these values. Among the genes, SOD2 had the highest total score. Calibration plot analysis showed a C-index of 0.870, indicating strong discriminatory ability (Figure 5B). The importance of the 4 hub genes was further assessed through ROC curve analysis and AUC values (Figure 5C). All 4 genes had AUC values above 0.5, confirming their robust

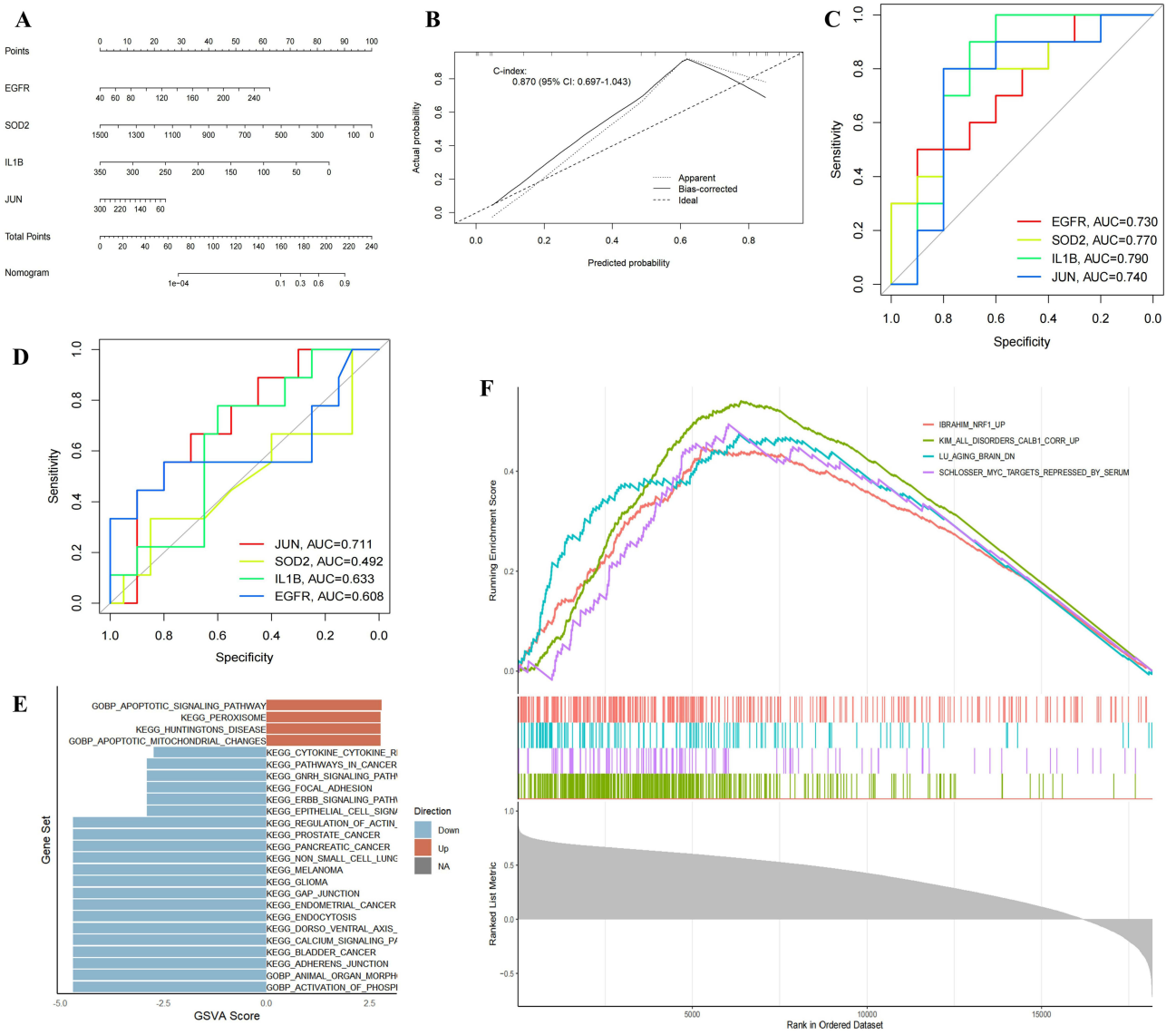

Figure 5 The Importance of four hub genes. (**A**) Nomogram and (**B**) Calibration plot were tested. (**C**) ROC curves analysis. (**D**) Validation with the external dataset GSE263180. (**E**) GSVA scores analysis. (**F**) The top 4 pathways in the c-JUN pathway analysis.

https://doi.org/10.2147/JIR.S544162

predictive capacity. Meanwhile, we selected an external dataset GSE263180 to validate the 4 hub genes, and except for SOD2, the AUC values of the others were all greater than 0.5 (Figure 5D).

GSVA was then performed to explore the pathway enrichment associated with the 4 hub genes (Figure 5E). The enrichment scores reflected the activity levels of related pathways in the samples. Additionally, GSEA single-gene analysis was conducted to examine potential pathways associated with JUN (Figure 5F, Figure S4A–D). The Normalized Enrichment Score (NES), which accounts for both gene set size and expression characteristics, was calculated. The IBRAHIM_NRF1_UP pathway had an NES of 1.924, and the IBRAHIM_NRF2_UP pathway had an NES of 1.86, both exceeding 1 (Figure S4D). These findings indicate significant upregulation or activation of the nuclear factor erythroid 2-related factor 2 (NRF1) and nuclear factor erythroid 2-related factor 2 (NRF2) pathways in the samples.

The results of Molecular Docking and MD Simulations

To investigate the relationship between the target genes and core compounds, the 4 hub genes (JUN, EGFR, IL1B, and SOD2) and their corresponding nine core compounds—paeoniflorigenone, ellagic acid, paeoniflorin, baicalein, baicalin, formononetin, eupatin, rhein, and aloe-emodin—were selected for molecular docking analysis using AutoDock software. Additionally, the two compounds with the highest degree values—beta-sitosterol and stigmasterol—were also included. The binding energy results from the molecular docking are shown in Figure 6B. The molecular docking results revealed that all 11 core active compounds interacted with the 4 target genes, with their minimum binding energies all below −6.4 kcal/mol. To visualize the interactions between the compounds and their target genes, PyMOL software was used to generate docking simulations (Figure 6A), focusing on the docking results of c-JUN (PDB ID: 1JNM) with rhein (−9.7 kcal/mol). Rhein engages in hydrogen Bond with ARG (A:270, B:271) and DG (C:211, C:210, D:310) within the internal cavity of c-JUN. Additionally, π-bond interactions were observed between rhein and adjacent ALA (A:266). Typically, binding energies with values lower than −5.0 kcal/mol are regarded as characteristic of stable intermolecular interactions, whereas those below −7.0 kcal/mol are deemed to indicate robust binding affinity.[25]

Next, we selected the c-JUN–rhein complex with the lowest binding energy for further analysis. The RMSD curve shows protein conformational fluctuations.[26] The values fluctuated between 0.2 and 0.7 nm during the simulation period, indicating minimal fluctuations in the protein structure from 0 to 100 ns, suggesting high binding stability (Figure 6C). This is because the protein may undergo structural adjustments in the initial simulation stage, reach a relatively stable dynamic equilibrium state later, but still have small - amplitude conformational fluctuations. RMSF analysis, which evaluates atomic-level stability, showed that protein fluctuations remained within a reasonable range during the simulations (Figure 6D), confirming the stability of the protein-ligand complex. The Rg values remained stable throughout the 100 ns simulation (Figure 6F), which measure the compactness of the receptor-ligand binding, and indicated that the complex retained its compact structure. (Figure 6F) The SASA, which reflects protein folding and structural stability, also remained stable throughout the simulation period (Figure 6E), further supporting the high stability of the complex. These findings verify that c-JUN forms highly stable interactions with rhein, supporting their potential as key pharmacological components in the therapeutic action of DYD. We also performed MD simulations on the c-JUN–baicalein complex (Figure S5A–E).

Results of in vitro Experiments

CETSA Proves Stable Binding Between c-JUN and Rhein

Given that ligand-target interactions can improve thermal stability, we employed CETSA to confirm the binding of rhein to c-JUN. We verified that c-JUN exhibited a significant increase in thermal precipitation at elevated temperatures when exposed to rhein in HMC3 and BV2 cells (Figure 7A, Figure S6A and B). The relative abundance of c-JUN in cells treated with compounds was significantly elevated compared to the control group across all assessed temperatures additionally. These findings validate that rhein directly associate with c-JUN, inducing thermal stabilization effects and providing further mechanistic understanding of their pharmacological actions.

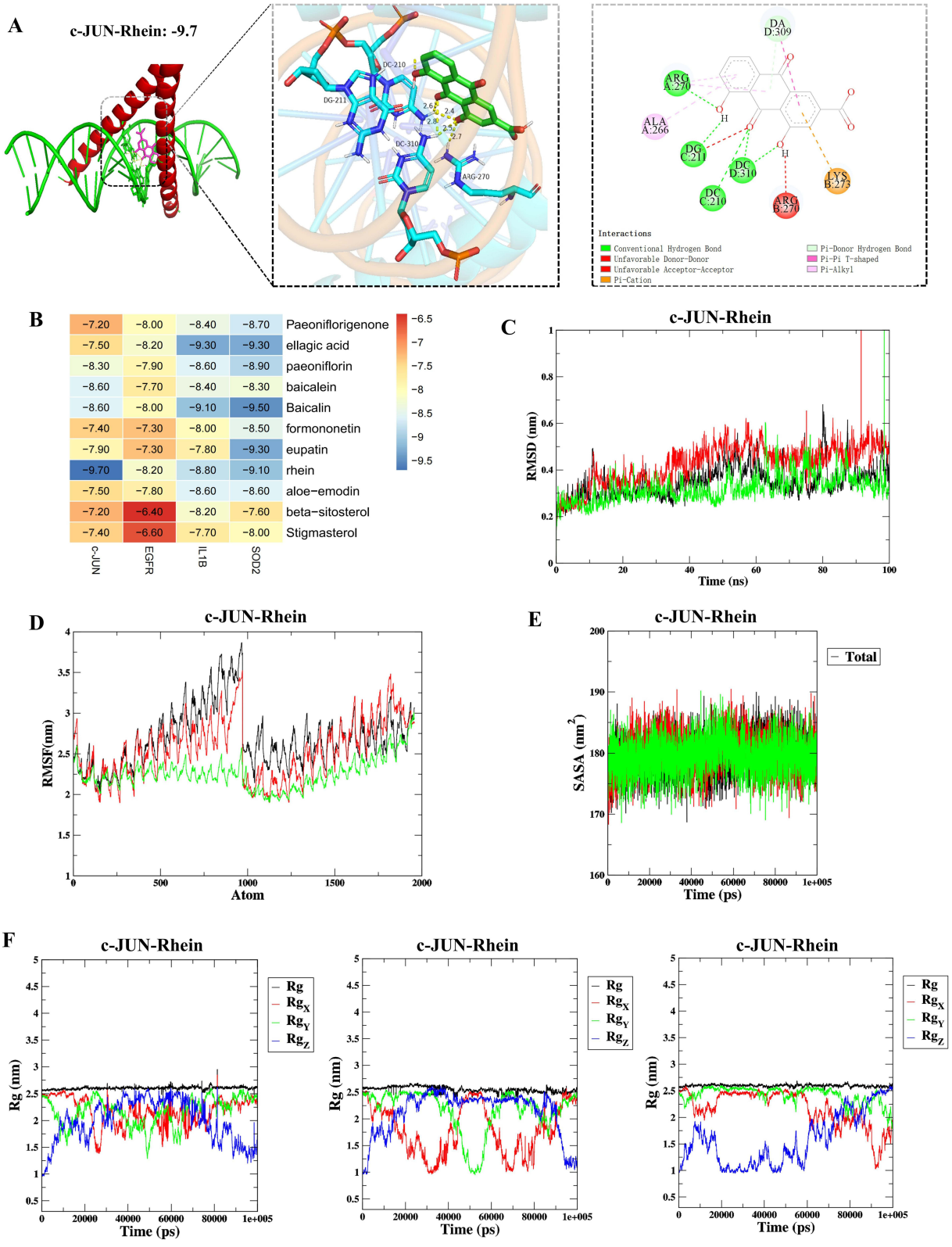

Figure 6 The results of Molecular Docking and MD simulations. (**A**) The docking results of rhein and c-JUN. (**B**) Molecular Docking Heat Map. The RMSD curve of c-JUN–rhein (**C**). The RMSF curve of c-JUN–rhein (**D**). The Rg curve of c-JUN–rhein (**F**). The SASA curve of c-JUN–rhein (**E**).

https://doi.org/10.2147/JIR.S544162

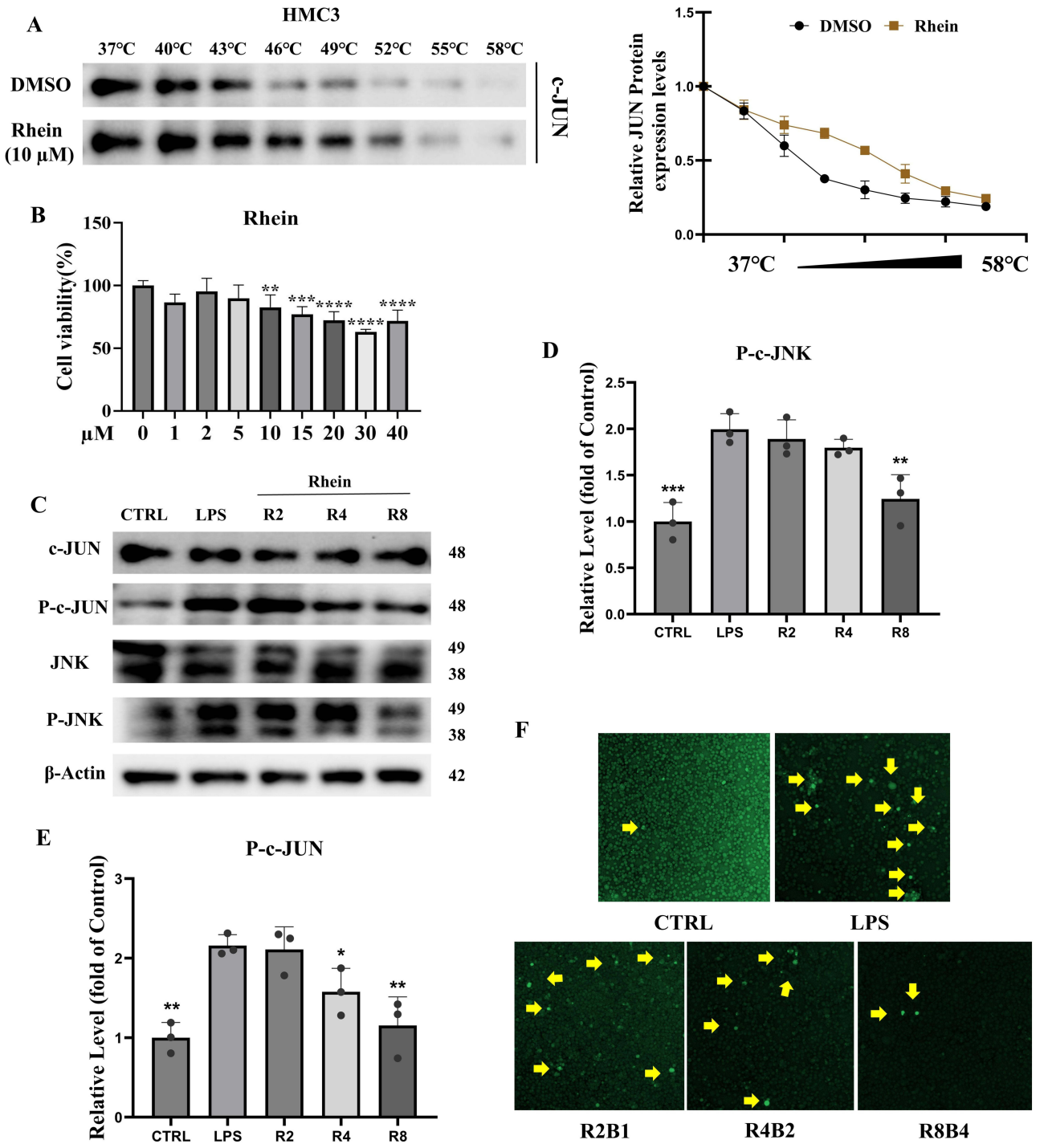

Figure 7 Results of in HMC3 cells experiments. (**A**) The immunoblot intensity of c-JUN in the presence and absence of rhein in the CETSA experiments. Representative images are shown. The relative intensity of c-JUN protein in the presence and absence of rhein, compared with that under increased temperature, was quantified in three independent experiments. (**B**) The Rhein results of CCK-8. *$p < 0.05$, **$p < 0.01$, ***$p < 0.001$, ****$p < 0.0001$ versus 0 group. (**C**) The results of Western blot (WB) for c-JUN, phosphorylated c-JUN (P-c-JUN), JNK, and phosphorylated JNK (P-JNK). (**D**) and (**E**) were relative levels of WB. *$p < 0.05$, **$p < 0.01$, ***$p < 0.001$, ****$p < 0.0001$ versus the LPS group. (**F**) Baicalein and Rhein Reduce ROS Levels. Each experiment was repeated three times.

Rhein Inhibits Cell Proliferation

The CCK-8 assay indicated that rhein hinders the proliferation of BV2 cells in a dose-dependent manner. Specifically, rhein demonstrated a significant inhibitory effect at concentrations above 10 μM ($p < 0.05$; Figure 7B), whereas baicalein markedly inhibited cell proliferation at concentrations exceeding 5 μM ($p < 0.05$; Figure S6C).

Rhein Inhibits the Phosphorylation and Activation of JNK/c-JUN

Previous studies have indicated that rhein can reduce neuroinflammation through the MAPK/NF-κB signaling pathway[27] thereby mitigating neuroinflammation and enhancing cognitive function. Nevertheless, the precise molecular targets and mechanisms responsible for these effects remain ambiguous. Therefore, we performed WB tests on HMC3 and BV2 cells to determine whether rhein alleviates neuroinflammation through the regulation of c-JUN target proteins. Based on the results of the CCK-8 assay, treatment groups were established: control group (CTRL), LPS-stimulated group (LPS), 2 μM Rhein (R2), 4 μM Rhein (R4), and 8 μM Rhein (R8). As illustrated in Figure 7C–E, the LPS group displayed a significant increase in the expression of P-c-JUN and P-JNK in HMC3 cells. The total protein levels of c-JUN and JNK were unchanged. Treatment with varying concentrations of rhein led to a pronounced reduction in the levels of P-c-JUN and P-JNK when compared to the LPS group, with no alterations in the overall amounts of c-JUN and JNK. When baicalein and rhein are combined, they produce a more significant reduction in the phosphorylation of JNK/c-JUN in BV2 cells than when either compound is used alone (Figure S6F–H). This proves that they may have potential as therapeutic agents for neuroinflammation related to SZ. The original WB images can be found in Supplementary FigureS1.

Then, we performed analysis across various treatment groups to assess the antioxidant effects. LPS stimulation resulted in a marked increase in ROS levels, as demonstrated in Figure 7F. Treatment with R2B1, R4B2, and R8B4 (Figure S6) conversely induced a dose-dependent decrease in ROS levels. These findings suggest that the combined administration of baicalein and rhein can effectively reduce the elevation of ROS caused by LPS. This will support their potential to alleviate neuroinflammation. On the other hand, to examine how compound regulates this inflammatory cascade, we evaluated the anti-inflammatory effect by measuring the mRNA expression levels of IL1B, TNF-α, and IL-6. RT-qPCR analysis revealed that following a 24-hour treatment with various drug concentrations, the mRNA levels of JUN, JNK, IL1B, TNF-α, and IL-6 were reduced compared to the LPS group after medication (Figure S6D and E). The reduction was greater with increasing doses of baicalein and rhein, showing a dose-dependent inhibition of LPS-induced inflammation.

These results imply that the drug may ease neuroinflammation by lowering ROS levels, JNK, and c-JUN phosphorylation, and the expression of pro-inflammatory cytokines.

Discussion

SZ is a complex and debilitating psychiatric disorder often accompanied by significant neuroinflammation. Pharmacological treatments mainly rely on dopamine receptor antagonists, but their effectiveness is limited. They also frequently cause severe side effects, such as metabolic disturbances.[28] Non-pharmacological approaches, such as psychotherapy, social interventions, and electroconvulsive therapy, offer certain benefits but are often limited by their high costs, restricting widespread use.[29] As a result, there is a pressing need for the development of novel therapeutic agents that offer enhanced efficacy with fewer side effects. TCM has drawn increasing interest due to its favorable safety profile and high tolerability.[6] DYD is a classical TCM formulation composed of various herbs with anti-inflammatory and antioxidant compounds. Paeoniflorin is a key active component of the herb *Paeonia lactiflora*, and has demonstrated the ability to reduce amyloid beta deposition, thereby alleviating LPS-induced cognitive dysfunction, particularly.[30] Despite the extensive clinical utilization of treatments targeting neuroinflammation associated with SZ, the precise molecular mechanisms remain unclear. Further research is necessary to clarify its pharmacological targets and therapeutic mechanisms.

Hence, in the context of this study, we used a comprehensive bioinformatics approach to screening biomarkers of SZNI. 871 DEGs were screened from the GSE26927, and 3090 SZ-relevant targets were identified from 5 publicly accessible databases. Among the 154 overlapping genes, marked correlations were identified between SZNI and plasma cells and activated mast cells through immunoinfiltration analysis. Plasma cells, essential in the production of antibodies, were significantly increased in the SZNI group, indicating immune response activation.[31] This can potentially lead to functional consequences as these immune cells, such as macrophages and microglia, are implicated in modulating the neuroimmune microenvironment during disease. Intersections between 533 DYD-related targets and endothelial cell targets yielded 17 intersecting targets, and 4 machine learning algorithms[32–35] "decreased" this to 4 hub genes (JUN,

SOD2, EGFR, IL1B). Molecular docking indicated that c-JUN showed abundant interactions with rhein, which binding energy was −9.7 kcal/mol. Further MD simulations confirmed that c-JUN–rhein complexes were stable during the simulations and validated the involvement of the interactions in the therapeutic mechanism of DYD in treating SZNI. Of the identified hub genes, c-JUN was given priority due to its well-established function in modulating inflammation, apoptosis, and neuronal damage.[36–38] These processes are closely linked to the cerebellar vermis in individuals with SZ.[39] These findings suggest that c-JUN may act as a key mediator of the neuroinflammation in SZ and that rhein may exert its therapeutic effects.

Transcription factor c-JUN (c-JUN) is a member of the key transcription factor activator protein 1 family,[40] and it is encoded by the proto-oncogene JUN. Up-regulation of c-JUN is a common event in the developing, adult as well as injured nervous system, and it exercises over neural cell death degeneration, gliosis inflammation plasticity repair.[41] The increased c-JUN N-terminal kinase (JNK) phosphorylation caused by the injury pattern[42] will further activate the phosphorylation of c-JUN and exacerbate neuroinflammation. Mammalian proteins bind to DNA through the dimeric basic leucine zipper domain, forming homodimers or heterodimers with Jun, thereby regulating gene transcription.[43] However, there have been no research reports so far on the relationship between c-JUN and SZNI under the influence of DYD. Therefore, targeting c-JUN is highly likely to be the best treatment strategy for SZNI. Our findings are consistent with previous reports that rhein has anti-inflammatory and ROS-reducing effects.[44–46] These activities are well known and not novel in themselves. The value of our study is in examining these effects in the context of SZNI and proposing possible molecular mediators, such as c-JUN. As our results are preliminary, they should be interpreted with caution. Although the machine learning models underwent regularization and cross-validation prior to data screening, limitations in sample size and the lack of independent validation mean that these findings are hypothesis-generating and require further experimental confirmation.

Based on the above results, the JNK/c-JUN signaling axis appears to be a significant target for rhein. They may exert their effects by directly binding to c-JUN or inhibiting the production of ROS, thereby obstructing LPS-induced phosphorylation and activation of JNK and c-JUN.[47] The phosphorylation site of Anti-P-c-JUN is S63, which aligns with the literature showing that JNK binds to the N-terminus of c-JUN and rapidly phosphorylates S63.[48] Studies have found that JNK activation of c-JUN has a substrate site preference, filtering out the influence of other MAPK kinases (ERK and p38).[49] Phosphorylated c-JUN acts as a transcription factor, facilitating the production of numerous pro-inflammatory cytokines.[50] By inhibiting this activation, rhein effectively suppresses neuronal inflammation.[45] ROS and inflammation, therefore, have a two-way interaction: high ROS contents induce inflammation, and high contents of pro-inflammatory cytokines stimulate ROS production even further.[51] Rhein may break the vicious cycle between ROS and inflammatory factors. Further studies are necessary to validate this hypothesis. That is, c-JUN protein must have a critical role in modulating inflammation and may prevent excessive activation of the immune system and therefore contribute to overall immunomodulation activity of rhein. Clinical studies have shown that DYD maintenance therapy significantly improves the clinical efficacy of cyclic psychosis, with minimal endocrine impact and high safety.[8,9] The in vitro experimental results in this study help clarify its possible clinical relevance.

Through this study, bioinformatics results predicted 4 hub genes and 11 core components, and demonstrated that c-JUN is a potential biomarker for the treatment of SZNI with DYD. In vitro experiments utilizing LPS to induce neuroinflammation have further substantiated our bioinformatics predictions. CETSA analysis revealed that rhein may directly interact with c-JUN, thus enhancing its thermal stability. The results align with the bioinformatics findings, indicating that rhein may be the core component of DYD, and c-JUN may serve as a potential biomarker in SZNI treatment that warrants further exploration. While the results provide initial insights into possible mechanisms, they should be interpreted as exploratory. Therefore, rhein could be a key small molecule in DYD targeting c-JUN for SZNI treatment, but the underlying molecular mechanisms of DYD still need further investigation.

While BV2 and HMC3 cells are widely used models for microglial function, they may not fully reflect the phenotypic and functional diversity of primary microglia or their interactions with other neural cell types in vivo. Future studies incorporating animal models or organoid systems may help to validate and extend these observations. Besides, multi-target and multi-pathway analysis with a specific emphasis will be performed. In future studies with siRNA knockdown and transfection with a plasmid, the mechanism of action of DYD in therapeutic use in SZNI will

become even clearer. The results in this work are also preliminary and should be interpreted with caution. The small sample size, limited validation, and some variability in the data mean that these findings are not definitive. Larger, independent cohorts and functional experiments will be required to confirm these results and clarify their biological significance. This study suggests, but does not confirm, that c-JUN may be involved in the effects of baicalein, rhein, or DYD in SZNI. Additional in vitro and in vivo studies are needed to verify whether DYD acts through this pathway in SZNI.

Conclusion

In this exploratory study, we used integrative bioinformatics and machine learning to prioritize c-JUN and 17 putative DYD–SZNI targets. Four candidate genes were selected by four algorithms and examined with nomogram analysis, GSEA, docking, and MD. Docking and MD suggested stable binding between c-JUN and rhein. Limited in-vitro assays (CETSA, WB, RT-qPCR, CCK-8, ROS) were consistent with reduced c-JUN activity but do not establish the mechanism or efficacy. These findings are preliminary and hypothesis-generating. Rhein should be viewed as a candidate compound for follow-up. Validation in independent datasets, orthogonal assays, and appropriate animal models is required before any clinical inference. The preliminary workflow and hypothetical conclusions of this study may provide a reference framework for future small-molecule discovery in the SZNI field.

Abbreviations

AUC, Area under the curve; BP, Biological processes; CC, Cellular components; CETSA, Cellular Thermal Shift Assay; CIBERSORT, Cell Type Identification by Estimating Relative Subsets of RNA Transcripts; CPSN, Core Component-Potential Target-Signaling Pathway Network; CR, Curcumae Rhizoma; Ct, Cycle threshold; DEGs, differentially expressed genes; DL, Drug-Likeness; DYD, Daying Decoction; GEO, Gene Expression Omnibus; GO, Gene Ontology; GSVA, Gene Set Variation Analysis; OB, Oral Bioavailability; GSEA, gene set enrichment analysis; KEGG, Kyoto Encyclopedia of Genes and Genomes; LASSO, Least absolute shrinkage and selection operator; MD, Molecular Dynamics; MF, Molecular functions; NES, Normalized Enrichment Score; NNET, Neural Network; PCA, Principal Component Analysis; PPI, Protein-Protein Interaction; PRR, Paeoniae Radix Rubra; RF, Random Forest; RG, Radius of Gyration; RMSD, Root Mean Square Deviation; RMSF, Root Mean Square Fluctuation; ROC, Receiver operating characteristic; ROS, reactive oxygen species; RRR, Rhei Radix et Rhizoma; SASA, Solvent-Accessible Surface Area; SGAs, Second-Generation Antipsychotics; SR, Sparganii Rhizoma; SVM, Support vector machine; SZ, Schizophrenia; SZNI, Schizophrenia-related Neuroinflammation; TCM, Traditional Chinese Medicine.

Data Sharing Statement

The open-access datasets are available through the following URL: GSE26927 (https://www.ncbi.nlm.nih.gov/geo/query/acc.cgi?acc=GSE26927); GSE263180 (https://www.ncbi.nlm.nih.gov/geo/query/acc.cgi?acc=GSE263180). Data will be made available on request.

Ethics Statement

This study did not involve any new experiments with human participants or animals conducted by the authors. All the data used in this study were obtained from publicly available databases with prior ethical approval and informed consent from the original investigators. According to Article 32, Items 1 and 2 of the Measures for Ethical Review of Life Science and Medical Research Involving Human Subjects (Ministry of Science and Technology of the People's Republic of China, 2023), research using legally obtained public data, or data derived from observing public behavior without intervention, is exempt from institutional ethical review. Therefore, this study was exempt from ethical approval by the authors' institutional ethics committee.

Acknowledgments

We thank all the researchers for participating in this study. This work was supported by the Shanxi Key Laboratory of Food and Drug Safety Open Subject "Study on the processing technology and safety evaluation of keel"; the Shaanxi Provincial Administration of Traditional Chinese Medicine; the Key Laboratory of Coal Environmental Pathogenicity and Prevention (Shanxi Medical University) Ministry of Education (China); the Shared Instrument Platform of the School of Pharmacy, Shanxi Medical University.

Author Contributions

All authors made a significant contribution to the work reported, whether that is in the conception, study design, execution, acquisition of data, analysis and interpretation, or in all these areas; took part in drafting, revising or critically reviewing the article; gave final approval of the version to be published; have agreed on the journal to which the article has been submitted; and agree to be accountable for all aspects of the work.

Funding

This work was funded by grants from the National Natural Science Foundation (81973411, China); the Scientific Research Funding Project for Returned Students in Shanxi Province (2020-084, China); the Key Research and Development Project of Shaanxi Province (2023-YBSF225, China); the 2023 Double First-Class Creation Action Project (2C622023009, China); Construction project of key research laboratory of traditional Chinese medicine in Shanxi Province (zyyyjs2024031, China); Traditional Chinese Medicine Innovation team of Shanxi TCM Administration (zyytd2024008, China).

Disclosure

The author(s) report no conflicts of interest in this work.

References

1. Kathleen A, Cynthia R, Chloe OC, Jason HM. Ion channels and schizophrenia: a gene set-based analytic approach to GWAS data for biological hypothesis testing. *Hum Genet*. 2011;131:373–391. doi:10.1007/s00439-011-1082-x
2. Chao L, Wang X, Mao X, et al. Metformin attenuates antipsychotic-induced metabolic dysfunctions in MK801-induced schizophrenia-like rats. *Psychopharmacology*. 2020;237:2257–2277. doi:10.1007/s00213-020-05524-w
3. Sophie R, Charreteur R, Peries M, et al. Abuse and misuse of second-generation antipsychotics: an analysis using VigiBase, the World Health Organisation pharmacovigilance database. *Br J Clin Pharmacol*. 2022;88:4646–4653. doi:10.1111/bcp.15420
4. Vítor F, Diana G, Ángela MV. Adipose tissue as a target for second-generation (atypical) antipsychotics: a molecular view. *BBA*. 2019;1865:158534. doi:10.1016/j.bbalip.2019.158534
5. Hongyong D, Ji X. Wendan decoction (Traditional Chinese medicine) for schizophrenia. *Cochrane Db Syst Rev*. 2017. doi:10.1002/14651858.CD012217.pub2
6. Xiaojie S, Fan F-C, Liu H, et al. Traditional Chinese medicine decoction combined with antipsychotic for chronic schizophrenia treatment: a systematic review and meta-analysis. *Front Pharmacol*. 2021;11:616088. doi:10.3389/fphar.2020.616088
7. Ningbo Y, Hu H, Li J, et al. Influence and mechanism of traditional chinese medicine intervention on cognitive dysfunction in patients with schizophrenia. *J Biobased Mater Bio*. 2023;18(57):51–57. doi:10.1166/jbmb.2024.2342
8. Kang Z, Guobao Y, Shenhan X. Experience in treating periodic psychosis with daying decoction. *Chinese Trad Pat Med*. 1978;1:30–33.
9. Li T. The efficacy of daying decoction in the maintenance treatment of cyclic psychosis and its influence on the endocrine system of patients. *J Emergency Traditional Chin Med*. 2016;25:2010–2012. doi:10.3969/j.issn.1004-745X.2016.10.061
10. Éimear MF, Golam MK. Cytokines in psychosis: from mechanism towards treatment and prediction. *Lancet Psychiat*. 2023;10:237–239. doi:10.1016/S2215-0366(23)00056-1
11. Hye-Rim C, Ji Sun H, Eun AK, Sung-Woo C, Seung-Ju Y. MiR-30a-5p and miR-153-3p regulate LPS-induced neuroinflammatory response and neuronal apoptosis by targeting NeuroD1. *J Biochem Mol Biol*. 2022. doi:10.5483/BMBRep.2022.55.9.061
12. Ping Z, Kun Z. TREM2 deficiency aggravates neuroinflammatory response and cognitive impairment via disease-associated microglia in Parkinson's disease. *Parkinsonism Relat Disord*. 2024. doi:10.1016/j.parkreldis.2024.106653
13. Yu-Feng T, Cheng-Hsien L, Shu-Fen H, Mao-Tsun L. Melatonin improves outcomes of heatstroke in mice by reducing brain inflammation and oxidative damage and multiple organ dysfunction. *Mediators Inflamm*. 2013;2013. doi:10.1155/2013/349280
14. Hongxiang H, Lu X, Wu C, et al. A review for the pharmacological effects of paeoniflorin in the nervous system. *Front Pharmacol*. 2022;13:898–955. doi:10.3389/fphar.2022.898955
15. Abdelmeniem E-B, Olumayokun AO. Formononetin inhibits neuroinflammation and increases estrogen receptor beta (ERβ) protein expression in BV2 microglia. *Int Immunopharmacol*. 2018;61:325–337. doi:10.1016/j.intimp.2018.06.016
16. Gong Jie Z, Ya Bin Z. Artificial Intelligence and Machine Learning in Clinical Medicine. *N Engl J Med*. 2023;388. doi:10.1056/NEJMc2305287

17. Sami P, Chithanathan K, Bisht K, et al. Microglia contribute to social behavioral adaptation to chronic stress. 2021;69:2459–73.doi:10.1002/glia.24053
18. Pascal FD, Fernando FS, Kashefi SN, et al. Common mechanisms in neurodegeneration and neuroinflammation: a BrainNet Europe gene expression microarray study. *J Neural Transm*. 2014;122:1055–1068. doi:10.1007/s00702-014-1293-0
19. Zhu D, Zhang X, Fang Y, et al. Identification of a lactylation-related gene signature as the novel biomarkers for early diagnosis of acute myocardial infarction. *Int J Biol Macromol*. 2024;282:137431. doi:10.1016/j.ijbiomac.2024.137431
20. Mohsen S, Paramita S-C, John P. Model-based ROC curve: examining the effect of case mix and model calibration on the ROC plot. *Med Decis Making*. 2021;42:487–499. doi:10.1177/0272989X211050909
21. HJ L, CH T, Bioengineering HTJA. Apoptosis-associated genetic mechanisms in the transition from rheumatoid arthritis to osteoporosis: a bioinformatics and functional analysis approach. *APL Bioeng*. 2024;8:046107. doi:10.1063/5.0233961
22. Wenhao L, Jing H, Peng-Peng R, Ying X, Jiang D-Y. Exploration of the mechanism of Zisheng Shenqi decoction against gout arthritis using network pharmacology. *Comput Biol Chem*. 2021;90:107358. doi:10.1016/j.compbiolchem.2020.107358
23. Ponder JW, Case DA. Force fields for protein simulations. *Annu Rev Biophys*. 2003;66:27–85. doi:10.1016/s0065-3233(03)66002-x
24. Fanfan H, Yu Z, Cheng Y, et al. Deciphering the pharmacological mechanisms of Scutellaria baicalensis Georgi on oral leukoplakia by combining network pharmacology, molecular docking and experimental evaluations. *Phytomedicine*. 2022;103:154195. doi:10.1016/j.phymed.2022.154195
25. Nian G, Lin W, An L, YuanKun X. Exploring the active ingredients and potential mechanisms of action of sinomenium acutum in the treatment of rheumatoid arthritis based on systems biology and network pharmacology. *Front Mol Biosci*. 2023;10:1065171. doi:10.3389/fmolb.2023.1065171
26. Brüschweiler R. Efficient RMSD measures for the comparison of two molecular ensembles. *Proteins*. 2003;50:26–34. doi:10.1002/prot.10250
27. Xin Q, Wang S, Huang J, et al. Rhein alleviates MPTP-induced Parkinson's disease by suppressing neuroinflammation via MAPK/IκB pathway. *Front Neurosci*. 2024;18:1396345. doi:10.3389/fnins.2024.1396345
28. Sameer J, Mandy J, Peter M. Schizophrenia. *Lancet*. 2022;399:473–486. doi:10.1016/S0140-6736(21)01730-X
29. Hongyu D, Ji X. Wendan decoction (Traditional Chinese medicine) for schizophrenia. *Cochrane Database Syst Rev*. 2016;6. doi:10.1002/14651858.CD012217.pub2
30. Hui Wen M, Jihyun K, Ho K, Ah Young L, Eun Ju C. Paeoniflorin attenuates lipopolysaccharide-induced cognitive dysfunction by inhibition of amyloidogenesis in mice. *Int J Mol Sci*. 2023;24:4838. doi:10.3390/ijms24054838
31. Mariane Nunes N, Maes M, Nunes SOV, et al. Activation of the immune-inflammatory response system and the compensatory immune-regulatory system in antipsychotic naive first episode psychosis. *Eur Neuropsychopharmaco*. 2019;29:416–431. doi:10.1016/j.euroneuro.2018.12.008
32. Jiun-Ruey H, Silke S. A review on longitudinal data analysis with random forest. *Brief Bioinform*. 2023;24:1–11. doi:10.1093/bib/bbad002
33. Xiaowei Y, Liangjun T, Lifang H. A robust least squares support vector machine for regression and classification with noise. *Neurocomputing*. 2014;140:41–52. doi:10.1016/j.neucom.2014.03.037
34. Gauruv B, Healy BC, Lokhande HA, et al. Early predictors of clinical and mri outcomes using Least Absolute Shrinkage and Selection Operator (LASSO) in multiple sclerosis. *Ann Neurol*. 2022;92:87–96. doi:10.1002/ana.26370
35. Alexander D, Martin K, Naomi A. Convolutional neural networks. *Nat Methods*. 2023;20:1269–1270. doi:10.1038/s41592-023-01973-1
36. Zhengcai M, Li J, Zhu J, et al. Jatrorrhizine retard obesity by modulating transcription factor c-Jun/c-Fos to downregulate Mmp12-mediated inflammation. *Int Immunopharmacol*. 2025;152:114405. doi:10.1016/j.intimp.2025.114405
37. Ana LC, Costa P, de Almeida LP, et al. Tf-lipoplex-mediated c-Jun silencing improves neuronal survival following excitotoxic damage in vivo. *J Control Release*. 2009;142:392–403. doi:10.1016/j.jconrel.2009.11.004
38. Candela D-C, et al. AP-1 (Activated Protein-1) Transcription Factor JunD Regulates Ischemia/Reperfusion Brain Damage via IL-1β (Interleukin-1β). Stroke. 2019;50:469–77. doi:10.1161/strokeaha.118.023739
39. Valentina KT, Alan DE, Svetlana VK. Increased expression of c-Jun transcription factor in cerebellar vermis of patients with schizophrenia. *Neuropsychopharmacol*. 2003;28:1506–1514. doi:10.1038/sj.npp.1300211
40. Yuanmeng Q, Zhao Y, Xia J, et al. Jun and JunB members of the AP-1 complex are potential therapeutic targets for silicosis. *Int J Biol Macromol*. 2024;277:134024. doi:10.1016/j.ijbiomac.2024.134024
41. Gennadij R. c-Jun Expression, activation and function in neural cell death, inflammation and repair. *J Neurochem*. 2008;107:898–906. doi:10.1111/j.1471-4159.2008.05684.x
42. Yana A, Mark TQ, Igor AS, Dmitriy NA. Alarmins and c-Jun N-Terminal Kinase (JNK) Signaling in Neuroinflammation. *Cells*. 2020;9:2350. doi:10.3390/cells9112350
43. Ewa MD, Reymer A, Kumar NV, et al. The ancillary N-terminal region of the yeast AP-1 transcription factor Yap8 contributes to its DNA binding specificity. *Nucleic Acids Res*. 2020;48:5426–5441. doi:10.1093/nar/gkaa316
44. Wen G, Xu B, Zhang Y, et al. Baicalin attenuates oxidative stress in a tissue-engineered liver model of NAFLD by scavenging reactive oxygen species. *Nutrients*. 2022;14:541. doi:10.3390/nu14030541
45. Yuyang L, Chen W, Ma J, et al. Rhein against Staphylococcus xylosus by interfering with respiratory metabolism and inducing oxidative stress. *Curr Res Food Sci*. 2024;8:100718. doi:10.1016/j.crfs.2024.100718
46. Hua L, Zhang T-A, Zhang W-Y, et al. Rhein attenuates cerebral ischemia-reperfusion injury via inhibition of ferroptosis through NRF2/SLC7A11/GPX4 pathway. *Exp Neurol*. 2023;369:114541. doi:10.1016/j.expneurol.2023.114541
47. Pei X, Yan L-J, Zhou H-L, et al. Emodin protects against lipopolysaccharide-induced acute lung injury via the JNK/Nur77/c-Jun signaling pathway. *Front Pharmacol*. 2022;13:717271. doi:10.3389/fphar.2022.717271
48. Christopher AW, Alvarez-Teijeiro S, Josue Ruiz E, et al. An intrinsic temporal order of c-JUN N-terminal phosphorylation regulates its activity by orchestrating co-factor recruitment. *Nat Commun*. 2022;13:6133. doi:10.1038/s41467-022-33866-w
49. Chad JM, Benjamin ET. Homing in: mechanisms of substrate targeting by protein kinases. *Trends Biochem Sci*. 2018;43:380–394. doi:10.1016/j.tibs.2018.02.009
50. Torben R, Raigel M, Sternberg C, et al. JUN mediates the senescence associated secretory phenotype and immune cell recruitment to prevent prostate cancer progression. *Mol Cancer*. 2024;23:114. doi:10.1186/s12943-024-02022-x
51. Carl N, Amy CB. Beyond oxidative stress: an immunologist's guide to reactive oxygen species. *Nat Rev Immunol*. 2013;13:349–361. doi:10.1038/nri3423